Controlling Light Localization and Light–Matter Interactions with Nanoplasmonics

Vincenzo Giannini, Antonio I. Fernández-Domínguez, Yannick Sonnefraud, Tyler Roschuk, Roberto Fernández-García, and Stefan A. Maier*

***N**anoplasmonics is the emerging research field that studies light–matter interactions mediated by resonant excitations of surface plasmons in metallic nanostructures. It allows the manipulation of the flow of light and its interaction with matter at the nanoscale (10^{-9} m). One of the most promising characteristics of plasmonic resonances is that they occur at frequencies corresponding to typical electronic excitations in matter. This leads to the appearance of strong interactions between localized surface plasmons and light emitters (such as molecules, dyes, or quantum dots) placed in the vicinity of metals. Recent advances in nanofabrication and the development of novel concepts in theoretical nanophotonics have opened the way to the design of structures aimed to reduce the lifetime and enhance the decay rate and quantum efficiency of available emitters. In this article, some of the most relevant experimental and theoretical achievements accomplished over the last several years are presented and analyzed.*

1. Introduction

The scattering of light by a dielectric particle is a problem that, despite being very old, hides some very rich physics. It was first treated theoretically by Lord Rayleigh, who considered the simple case of spheres much smaller than the wavelength of light at the end of the nineteenth century.[1] His research led to the understanding of many phenomena related to light diffusion. For instance, in one of his most famous works,[2] he showed that the scattering of light by a diluted gas follows a ω^4 law, where ω is the angular frequency of the incoming radiation. This means that at high frequencies (blue), light is scattered more efficiently by air molecules than at low frequencies (red). This simple law provides an elegant explanation on the blueness of the sky, the redness of the sunset, or the yellow color of the sun.

Dr. V. Giannini, Dr. A. I. Fernández-Domínguez, Dr. Y. Sonnefraud, Dr. T. Roschuk, Dr. R. Fernández-García, Prof. S. A. Maier
Department of Physics
Imperial College London
London SW7 2AZ, United Kingdom
E-mail: v.giannini@imperial.ac.uk

DOI: 10.1002/smll.201001044

Two decades later, a more general analysis, not limited to small particles, was performed by Mie.[3] He established the first full analytic study of light scattering by spherical particles. Expanding a plane wave in spherical waves and matching the boundary conditions on the object surface, Mie was able to obtain the scattering and the absorption cross sections of spheres of any arbitrary size.

Since the work of Mie, the spherical geometry is the only one for which an exact analytical theory describing the scattering of light by particles exists. Excluding the use of numerical methods, the treatment of any other shape requires the introduction of different levels of approximation. Thus, based on the Rayleigh and Mie approaches, Gans extended the theoretical framework to ellipsoidal geometries, demonstrating that the optical properties of metal nanoparticles (NPs) depend strongly on their shape.[4] This explained why the color of a solution containing ellipsoidal NPs changes when the ratio between the particles' axes is varied.

Although theoretical solutions explaining the scattering of light by metal NPs have only been developed over the last century and a half, the characteristic color of metal NPs has been exploited since the days of the Roman Empire. As early as a couple of centuries BC, NPs were used as colorants in cloths, stained glasses, or ceramics. Obviously, it was not

small NANO MICRO

known that the origin of such intense colors was due to the presence of tiny metallic particles, as the length scale involved in the scattering of light by NPs (1 nm–1 μm) is many orders of magnitude smaller than everyday human experience (from 1 mm upwards). As a result of this, the research field lost momentum after Gans' work, largely because of the impossibility of building colorful nanometric particles in a controlled manner.

Over the past few decades, however, recent extraordinary advances in fabrication and characterization on the nanoscale have given rise to a renewed interest in the scattering properties of metal NPs. Advances in single-particle spectroscopy, such as confocal microscopy,[5,6] dark-field microscopy,[7] and scanning near-field optical microscopy (SNOM),[8–11] combined with new developments in highly sensitive detectors, including avalanche photodiodes (APDs) and photomultiplier tubes (PMTs), have allowed us to interact with and study structures on this scale.

The emergence of nanophotonics as a fruitful research field over the past decade has led to a deep understanding of electromagnetic phenomena occurring on the nanoscale and to the identification of plasmonic resonances as the key factors controlling the optical response of metallic nanostructures.[12–20] Today, it is well known that the interaction of light with noble metals, such as gold or silver, is mainly driven by the coherent oscillations of the quasifree electrons (plasmons) in the conduction band.[15,21] In a simple picture, when light encounters a metallic NP, the interaction of the electromagnetic field with the electrons in the metal causes them to abandon their equilibrium positions, giving rise to a surface-density charge on the nanostructure. The system then tends to revert to its minimum-energy configuration and the electrons try to return to their equilibrium positions, leading to the creation of charge-density oscillations within the NP. When the characteristic frequency of these charge oscillations coincides with that of the external excitation, the response of the metal nanostructure becomes resonant in nature. These are the so-called localized surface plasmon resonances (LSPRs), where the term localized is used to distinguish them from the bounded plasmonic modes supported by extended metal surfaces such as a semi-infinite plane.[18]

Currently, metal NPs are playing a fundamental role in the development of nano-optics. They are key structures allowing access to length scales below the diffraction limit,[21–23] which overcomes the main limitations of classical optics. LSPRs have the striking ability to squeeze light into nanometer dimensions, producing large local enhancements of electromagnetic energy, which allows the manipulation of light–matter interactions at the nanoscale. In this sense, they work in a similar way as antennas do in the radio and telecommunication regimes, although at optical frequencies.[1,19] For this reason, metal NPs are also called nanoantennas or optical antennas.

In this context, the interplay between emitters, such as fluorescent or dye molecules or quantum dots, and LSPRs supported by nanoantennas has received a great deal of attention recently. The radiative properties of emitters can be dramatically modified by the near-field interaction with surface plasmons.[13,20,24–26] A clear example of enhanced light–matter interaction is the so-called surface-enhanced Raman scattering (SERS).[25] In SERS spectroscopy, the Raman emission of molecules located in the electromagnetic near-field of localized surface plasmons is enormously enhanced, allowing even single-molecule detection.[25–27] More recently, a growing interest is being devoted to another phenomenon related to the interaction of LSPRs and emitters. Similarly to quantum-electrodynamics cavities, LSPRs can modify the decay rate of an emitter placed in their vicinity. This enables one to act on the emitters, obtaining faster or slower decay rates, and also to improve the quantum yield for emitters with low intrinsic efficiencies. LSPRs are particularly promising because the decay-rate variations are stronger for smaller mode volumes and surface plasmons confine electromagnetic fields in deeply subwavelength dimensions.[28,29]

Finally, let us stress that apart from the multiple potential applications of LSPRs supported by metal NPs in technological areas such as sensing, spectroscopy, and imaging, the interplay of emitters with plasmonic resonances offers a new scenario in which it is possible to study light–matter interactions in nanometric systems at a fundamental level.

The aim of this article is to provide a general overview on the most relevant concepts that are driving the development of nanoplasmonics in metal nanostructures. It is organized as follows: In Section 2, we describe how plasmonic effects govern light–matter interactions in nanometric metallic particles at optical frequencies. In Section 3, we introduce two concepts which have recently provided novel modulation strategies of localized plasmons: dark modes and Fano resonances. Section 4 is dedicated to reviewing how the radiative properties of emitters can be drastically modified by the presence of metallic nanostructures in their vicinity. To conclude, future prospects and perspectives of the field are discussed in Section 5.

2. Plasmonics and Nanoparticles

Tailoring the shapes and the dimensions of metal NPs is a fundamental ingredient in order to control and tune plasmonic resonances. The intense research effort devoted during the last decade to the development of efficient nanofabrication processes today allows the manipulation of nanoparticle geometries at the nanometer scale. Several techniques have been developed that eased the fabrication of bespoke structures. Some are based on chemical shape-controlled synthesis.[30,31] Others rely on new nanofabrication tools: electron-beam lithography,[32,33] nanoimprint lithography,[34,35] or focused ion beam (FIB) milling[36] using liquid metal-ion sources.[37] The emergence of all these nanofabrication techniques has made it possible to engineer the electromagnetic response of noble-metal nanostructures to an unprecedented accuracy.

The high accuracy of current nanostructure design is clearly illustrated by **Figure 1**. Panels a and b show scanning electron microscopy (SEM) images of arrays of silver nanobars[31] and nanoprisms,[30] respectively, of sizes below 100 nm, built by chemical shape-controlled synthesis. On the other hand, Figure 1c,d correspond to SEM images of two single gold 100-nm-size particles obtained using electron-beam

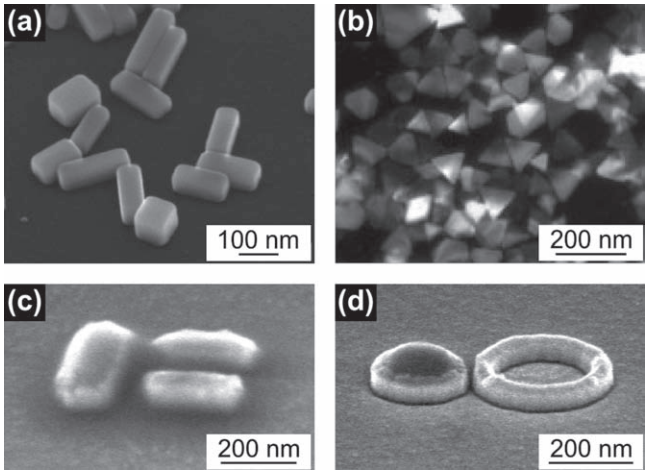

Figure 1. SEM images of examples of designer nanostructures. a) Silver nanobars chemically synthesized, adapted with permission.[31] Copyright 2007, American Chemical Society. b) Silver nanoprisms generated from nanospheres by photoconversion, adapted with permission.[30] Copyright 2001, Association for the Advancement of Science. c) Dolmen-shaped and d) disk near-ring-shaped gold plasmonic resonators produced by e-beam lithography, using an inverted resist process. Images courtesy of N. Verellen, and structures are the same as those presented previously.[6] Copyright 2009, American Chemical Society.

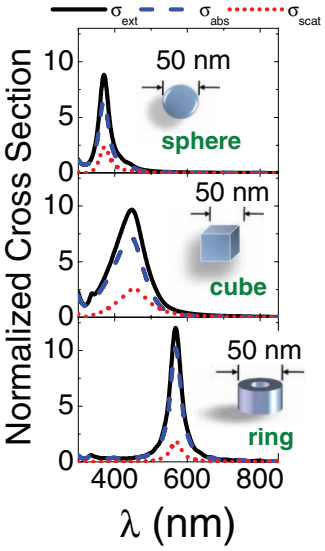

Figure 2. Normalized extinction, absorption, and scattering cross sections for three different Ag nanoparticles in vacuum. Upper and middle panels correspond to a 50-nm-diameter sphere and a 50-nm-side cube, respectively. Lower panel shows the cross sections for a 20-nm-high ring with inner and outer radii of 15 and 25 nm, respectively.

lithography and subsequent metal milling: a nanodolmen and a dimer composed of a nanoring and a nanodisc. All these nanostructures have relatively simple shapes but current fabrication techniques make it possible to explore light–matter interaction in more complex geometries, such as bowties, stars, flowers, or rings.[31,38–43]

Two main effects are observed when LSPRs are excited in metal NPs. The metal structure acts on part of the electromagnetic energy carried by the incident light by dissipating it in the form of heat within the NP or reradiating it again into free space. These two mechanisms correspond to the well known optical concepts of absorption and scattering, respectively, and their interplay is completely dictated by the particle geometry and the intrinsic dielectric response of the metal. We can write the absorbed and scattered powers in terms of effective cross sections intrinsic to the metal NP. This simple concept, the effective cross section(s), σ, enables us to visualize NPs as optical antennas, whose interaction with light is described by the effective interception area they present to the incident radiation. In this picture, the total energy removed from the incoming light, that is, the sum of the absorption plus the scattering contributions, is given by the so-called extinction cross section. If I is the incident intensity (power flow per unit area) and P_{abs} and P_{sca} are the absorbed and scattered powers, the corresponding cross sections σ_{abs} and σ_{sca}, respectively, are therefore defined as

$$\sigma_{abs} = P_{abs}/I, \qquad \sigma_{sca} = P_{sca}/I, \tag{1}$$

and the total effective area (the extinction cross section) that the light experiences when interacting with the nanoparticle is $\sigma_{ext} = \sigma_{abs} + \sigma_{sca}$.

The excitation of LSPRs can lead to an increase of the effective area up to several times the physical cross section of the nanoparticle. This effect is shown in **Figure 2**, which plots the scattering (red dotted line), absorption (blue dashed line), and extinction (black solid line) cross sections for different silver-NP shapes (see figure insets) within the visible range. Note that in the three cases, the system is illuminated under normal incidence. For comparison, the cross sections are normalized to the physical area of the nanoparticle. It can be seen that at resonance the effective size of the scatterer can be more than 10 times larger than its actual area, which is a clear indication of the strong interaction that takes place between the NP and the incident light, mediated by localized surface plasmons.

Figure 2 also demonstrates the important role that shape plays in LSPR excitations. The top panel shows the narrow peak that appears in σ for a 50-nm-diameter spherical NP, which is linked to the dipole resonance that it sustains at 370 nm. In contrast, a cubic NP of 50-nm side (middle panel) presents a broader maximum, also associated with a dipole resonance around 430 nm, that is redshifted with respect to the sphere case, and a small peak due to the quadrupolar resonance around 350 nm. The dipole resonance redshift with respect to the spherical case can be related to the fact that it is possible have charge accumulation near the structure edges. This maximizes the distance among induced charges of the same sign, reducing the repulsion between them, and leading to an energy lowering of the LSPR excited in the system. This effect can be also observed in Figure 2c, which plots the different cross sections for a 20-nm-high ring NP with outer and inner radii of 25 and 15 nm, respectively.

Metallic rings have a simple but highly tunable geometry and, as Figure 2 shows, they present high and narrow cross-section peaks, which make them very good candidates

small NANO MICRO

for nanoantennas due to their strong interaction with free-space radiation. Note that for the three cases considered here, a very small part of the incident energy is scattered by the NP and absorption dominates the cross section. This is the case for metal particles much smaller than the wavelength (sizes below 100 nm for visible frequencies), whereas, for larger sizes, it is the scattering contribution that dominates the cross section of the structure.

As will be shown in the following sections, an efficient antenna must not only have a large and spectrally tunable cross section but also give rise to a high field enhancement in its vicinity. A simple plasmonic structure featuring these two characteristics is a metallic nanobar (see **Figure 3**). The properties of plasmonic resonances in this geometry are mainly controlled by the length of the NP along the direction parallel to the polarization of the incident light. For this reason, this structure provides us with a simple picture describing the fundamental physics behind LSPRs. If we think of the nanobar particle as a Fabry–Perot plasmonic cavity (see Figure 3a), its length, L, must contain a half multiple of the effective wavelength of the fields, λ_{eff}, within the metal at resonance, that is,

$$L = n\lambda_{eff}/2, \tag{2}$$

where $n = 1, 2, \ldots$ is an integer and λ_{eff} is related to the wavelength λ of the external incident field by the relation[45]

$$\lambda_{eff} = n_1 + n_2\lambda/\lambda_p, \tag{3}$$

where n_1 and n_2 are constants that depend on the geometry and the dielectric properties of the background and the particle and λ_p is the metal plasma wavelength (which for most metals lies in the ultraviolet regime). Equation 3 reflects the momentum increase that the incoming photons experience when interacting with the collective electron oscillations within the metal NP. For decreasing λ, and as we approach λ_p, this effect becomes more prominent, which translates into a drastic reduction of the effective wavelength at the metal structure, which can be one order of magnitude smaller than the free-space wavelength.[19]

The first (and most intense) plasmonic resonance ($n = 1$) sustained by metallic nanobars satisfies the relation $L = \lambda_{eff}/2$ (half-wave resonance). For a fixed length, this condition gives the lowest LSPR supported by the system. Figure 3a shows the extinction cross section and the electric-field intensity for this resonance in the case of a gold nanobar with dimensions of 400 nm × 100 nm × 50 nm deposited on a glass substrate. The electric field external to the nanoparticle has a maximum at the ends. In contrast, the electric field inside has a maximum at the middle and presents two minima at the structure ends (see inset of Figure 3a). Correspondingly, the induced charges within the NP (given by the divergence of the instantaneous electric field) will present, as expected, a dipolar distribution. These simple arguments can be also applied to higher multipole resonances, which allow us to predict the associated field pattern and induced charge distribution (see Figure 3a). In particular, note that for higher multipole resonances (i.e., n = 2 and n = 3), one and two minima (nodes) are presented respectively, in accordance with the Fabry–Perot cavity picture (see the near-field map of Figure 3a). Another remarkable characteristic of these resonances is the electric-field intensity enhancement that can be bigger than 10^2 times the incident-field intensity (red color in the near-field map of Figure 3a).

It is of particular interest to analyze how the properties of a dipole nanoantenna are modified when it is cut at its middle point, that is, when a small gap is opened along its length L (see Figure 3b). Within the gap, the component of the electric field parallel to L, which governs the total field amplitude, is uniform. Due to the continuity conditions of the electric displacement at the gap interfaces, the magnitude of the electric field will be proportional to the ratio between the dielectric constant of the nanostructure and the background,

$$E_{gap} = \frac{\varepsilon_{NP}}{\varepsilon_b} E_{NP}, \tag{4}$$

where E_{NP} stands for the electric field inside the metallic NP and near the gap. For noble metal nanoantennas operating at visible and near-infrared wavelengths, this means that intensity enhancements, $|E_{gap}|^2/|E_0|^2$ (where E_0 is the incident electric field), of the

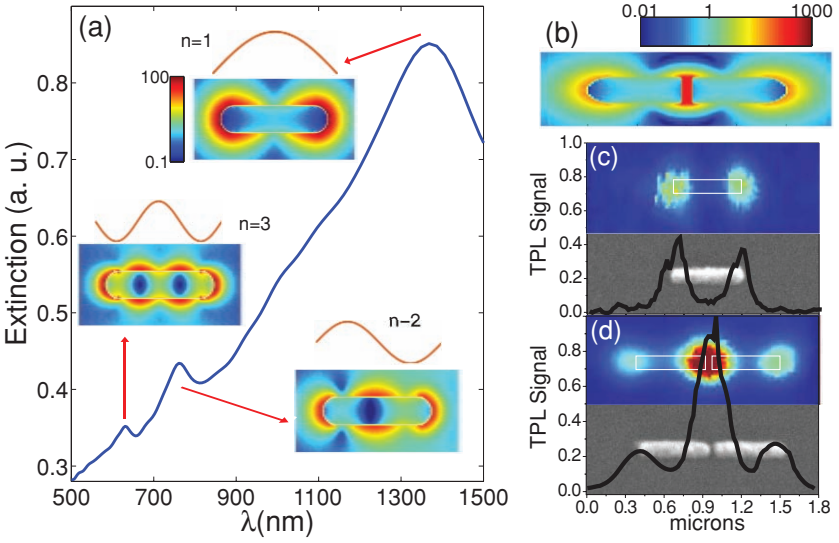

Figure 3. Plasmonic resonances in a gold nanobar. a) Extinction cross section (blue line) of a gold nanobar with dimension 400 nm × 100 nm × 50 nm deposited on a glass substrate. Three different resonances are excited, one dipolar, $n = 1$, and two multipolar, $n = 2$ and $n = 3$. The respective near-field enhancement $|E|^2/|E_0|^2$ is shown on a logarithmic colorscale. b) The electric-field intensity enhancement $|E|^2/|E_0|^2$ for two antennas with the same dimension as (a) but with a gap of 20 nm. c,d) Experimental hotspot map for a single nanoantenna (c) and for two coupled nanoantennas by means of two-photon luminescence measurements (d). Adapted with permission.[44] Copyright 2008, American Physical Society.

order of 10^3 or higher can be obtained for gap widths of a few tens of nanometers, as shown in Figure 3b. If a light emitter is located within the gap of such antenna, it will be excited very efficiently due to the ability of the antenna to concentrate the electromagnetic energy carried by the incident radiation within the gap. In Section 4, we will see that the presence of the metallic nanostructure also modifies the local density of photonic states within the antenna gap, which drastically affects the radiative properties of any emitter placed within its vicinity. These two independent mechanisms mediated by metallic NPs provide us with a very suitable strategy to manipulate the emission- and decay-rate properties of light emitters.

Recently, a technique based on the nonlinear responses of nanoantennas, that is, two-photon-excited luminescence (TPL), has been used in order to map the hot spots in nanoantennas.[44] Figure 3c shows the TPL microscopy image obtained for a 500-nm-long single nanobar. Figure 3d corresponds to a composite nanoantenna in which a 50-nm gap is opened between two 500-nm-long nanobars. Both antennas were illuminated with monochromatic light (730 nm) polarized along their long axis. We can observe hot spots appearing at the extremes of the metal structures. However, the composite antenna presents an even larger field enhancement at the gap, in very good agreement with the theoretical calculations rendered in Figure 3b. Recently, the fundamental role played by the gap in composite nanobar antennas has been studied experimentally in the infrared regime and in a new class of nanoscale optical switches proposed consisting of a plasmonic nanoantenna loaded with a photoconductive semiconductor material.[46a,b]

3. Dark Modes and Fano Resonances

Due to the strong radiative character of oscillating electric dipoles, dipole LSPRs are excited very efficiently by free-space radiation (plane waves). Hence, light–matter interactions occurring in deeply subwavelength structures are usually dominated by the electric dipole moment induced in the system by the incident fields. For this reason, the dipole plasmonic resonances (the lowest in energy) supported by metallic NPs are usually known as bright modes. However, Maxwell's equations predict the existence of higher multipole modes that are dipole inactive and that hardly couple to light. In contrast to dipole bright modes, these higher-order resonances are termed dark modes. Let us emphasize that the only mechanism that allows the excitation of these higher-order resonances by free radiation are retardation effects, whose origin is the slow response of metallic plasma electrons to the external excitation. This means that higher-order modes can only be excited in metallic NPs big enough for these retardation effects to be relevant. Note that, even in this case, high-multipole LSPRs only couple to incident fields with the same symmetry properties.[47] The difficulty of probing dark modes through optical methods has led to the recent appearance of several experimental works in which these plasmonic resonances are studied by means of electron-energy-loss spectroscopy techniques.[48,49]

The nature of dark modes can be easily understood by considering a simple system, the plasmonic excitations appearing in two small metallic spheres placed close to each other. The interaction between the LSPRs supported by each sphere can be interpreted by means of the hybridization model proposed by Prodan and co-workers.[50] This elegant theoretical approach establishes the analogy between bound electromagnetic modes in composite metallic structures and electronic orbitals in molecules. Molecular states result from the overlapping of the atomic orbitals involved in the chemical binding. Similarly, LSPRs of complex structures can be described through the electromagnetic coupling of the modes supported by the isolated elements forming them. **Figure 4**a sketches a simple energy diagram for the hybridized modes sustained by a dimer comprising two metallic spheres. For deeply subwavelength systems, the energy levels are dictated by the electrostatic interaction between the charges induced in the spheres. Thus, the configuration that maximizes the distances among charges of opposite sign corresponds to the lowest energy (note that some dimer modes have even higher energy than the isolated ones). Importantly, as can be seen in Figure 4a, the lowest composite LSPR also presents the largest net dipole moment. This constitutes a very bright mode, as it interacts strongly with incoming radiation. All the higher plasmonic

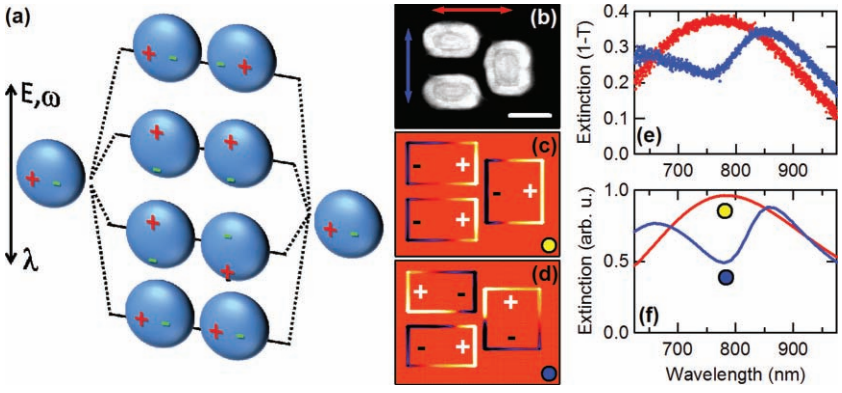

Figure 4. Dark modes and Fano resonances. a) Plasmon hybridization in spherical nanoparticles. The dipole plasmon of individual spherical particles is three-fold degenerate (along the three space axes). When two particles are close enough to interact, the dimer formed exhibits modes that originate from the hybridization of the modes in the single particles. The lowest energy mode is bright, with a large dipole moment. The highest energy mode has zero dipolar moment and does not couple to radiation (dark mode). b) SEM image of a dolmen structure. Charge distribution in the dolmen when illuminated with a polarization c) along and d) perpendicular to the symmetry axis of the structure (c.f., the red and blue arrows in (b), respectively). e) Confocal extinction cross section of the dolmen for the two main polarizations. f) Extinction cross sections computed by finite-difference time-domain (FDTD) calculations for this structure. When the exciting field is perpendicular to the symmetry axis of the structure, the quadrupolar (dark) mode of the dimer interacts destructively with the dipole of the monomer, opening a transmission window with a nearly symmetric Fano shape. Adapted with permission.[6] Copyright 2009, American Chemical Society.

NANO MICRO small

modes sustained by the dimer are darker (less bright or completely dark), as their net dipole moment is smaller or zero.

Very rich physics arises when nanoantennas supporting bright (dipole) modes are placed in the vicinity of nanostructures sustaining dark modes. Dipole resonances suffer strong radiative damping, which makes them very broad in frequency. In contrast, higher multipole (dark) resonances are usually spectrally narrow, their width being constrained only by absorption losses within the metal. The interaction of sharp and broad NP resonances gives rise to asymmetric spectral features that, due to their similarities with profiles appearing in autoionization spectra, are known as Fano-like resonances.[51] With this framework, the interaction between narrow (discrete) and broad (continuum) plasmonic resonances gives rise to asymmetric profiles in which peaks (dips) can be linked to the constructive (destructive) interference of two distinct excitation channels of the composite mode.

Figure 4b shows an SEM image of a metallic nanostructure supporting Fano resonances.[6] It comprises three gold nanobars of similar dimensions (≈100–200 nm) arranged in a dolmen-like fashion. When the structure is illuminated from the top with light polarized along the long axis of the two parallel nanobars (red arrow), a broad maximum is observed at 780 nm in the measured extinction spectrum, plotted in red in panel e of Figure 4. Its origin is the coherent superposition of the dipole resonances excited in the parallel nanobars. However, when the incident polarization is rotated 90° (blue arrow), a narrow dip develops in the spectrum at the same position (blue dots) and a Fano profile is formed. This effect can be attributed to interactions between the bright dipole mode supported by the monomer parallel to the polarization direction and a dark quadrupolar mode excited in the dimer oriented perpendicularly. The experimental results are corroborated by the numerical finite-difference time-domain (FDTD) calculations shown in Figure 4f. Figure 4c,d plots the instantaneous charge distribution at resonance for both polarizations, which validates the physical picture of coupled dipoles presented above and at higher-order resonances. It is important to stress that, due to symmetry constraints, the quadrupolar mode supported by the dimer could never be excited at normal incidence and that it is the presence of the monomer which permits the coupling in the near field.

Remarkably, when bright and dark modes overlap in frequency, Fano resonances can evolve into a sharp and deep extinction dip, which makes the supporting nanostructure "transparent" within a narrow frequency range. This phenomenon is known as plasmonic-induced optical transparency and has been recently predicted theoretically by Zhang et al.[52] and experimentally verified by Liu and co-workers.[53] Plasmonics nanostructures with Fano profiles show interesting properties, such as large refractive-index sensitivity or high tunability, which make them good candidates for sensing applications.

4. Decay-Rate Emission Close to a Nanoantenna

As Purcell pointed out in 1946, the radiative properties of a given emitter (a fluorescent molecule, for instance) are not intrinsic to it but also depend on its environment. This simple statement lies at the core of the so-called Purcell effect,[54] which several decades ago allowed the control of stimulated-emission phenomena and opened the way to the development of current laser technology. The simplest theoretical framework we can use to model the decay rate of any fluorescent emitter is the so-called Lorentz harmonic oscillator.[13,55] Despite its classical character, it gives deep physical insight into the problem and has demonstrated extremely good prediction capabilities, in very close agreement with experimental results. Within this approach, the transition dipole moment induced in a weakly excited (below saturation) quantum emitter is modeled by a classical electric dipole, μ, whose equation of motion reads

$$\frac{d^2\mu}{dt^2} + \omega_0^2\mu + \gamma_0\frac{d\mu}{dt} = \frac{e^2}{m}[\mu^* E_l]\frac{\mu}{\mu^2}, \quad (5)$$

where ω_0 and $\gamma_0 = 1/\tau_0$ are the resonant frequency and the decay rate (inverse lifetime), respectively, of the emitter in the absence of any excitation. The term on the right hand side of Equation 5 takes into account the interaction of the electric dipole with the local electric field, E_l, projected along the dipole axis and evaluated at the position of the emitter. In the absence of any external illumination, E_l corresponds to the electric field emitted by the dipole itself, which is then backscattered by the surrounding medium. The presence of this term in Equation 5 opens the way to manipulate the radiative properties of quantum emitters by placing engineered metallic nanostructures (nanoantennas) in their vicinity.

The excitation of an isolated fluorescent molecule is given by the homogeneous solutions of Equation 5. This process is completely governed by the decay rate, γ_0, which describes the amplitude decay suffered by the transition dipole in time. We can identify two contributions to this overall decay: γ_{r0}, which takes into account the electromagnetic energy that is released in the form of free radiation, and γ_{nr0}, which is linked to nonradiative phenomena, such as, for example, the energy lost as heat due to the excitation of the rotational and vibrational levels of the molecule. In order to measure the efficiency of the emitter we introduce the intrinsic quantum yield,

$$\eta_0 = \frac{\gamma_{r0}}{\gamma_0} = \frac{\gamma_{r0}}{\gamma_{r0} + \gamma_{nr0}}, \quad (6)$$

which represents the probability that an (already) excited fluorescent molecule emits one photon. As discussed above, the Lorentz oscillator model shows that the emission of light by a fluorescent molecule is altered by the presence of metallic nanostructures in its vicinity. This effect modifies the quantum yield of the molecule which, without loss of generality, can be written as

$$\eta = \frac{\gamma_r}{\gamma} = \frac{\gamma_r}{\gamma_r + \gamma_{nr} + \gamma_{nr0}} \quad (7)$$

where $\gamma = 1/\tau$ is the total decay rate and τ is the transition lifetime. We can identify three different decay channels in the system now: the radiative rate, γ_r, the nonradiative rate due to

metal absorption losses in the environment, γ_{nr}, and γ_{nr0}, the nonradiative rate intrinsic to the emitter.[55]

A deeper and clearer understanding of light–matter interactions is possible if we go a step further in our theoretical description and treat the molecular emitter as a quantum entity. Thus, the decay rate associated with the spontaneous emission process that accompanies the electronic transition between two molecular energy states is given by the Fermi's golden rule

$$\gamma_r = \frac{2\pi}{\hbar^2} \left| M_{if} \right|^2 \rho(\omega), \tag{8}$$

where M_{if} is the transition-matrix element between the initial molecular state $|i\rangle$ and the final state $|f\rangle$ (lower in energy), and $\rho(\omega)$ is the photonic local density of states (LDOS).[56] The environment of an emitter can modify the LDOS and therefore its emission properties.

For example, in free space and in the absence of any preferred dipole direction and without any incident field, the transition-matrix element averaged over all directions is $\left| M_{if} \right|^2 = |\mu|^2 \hbar\omega/6\varepsilon_0$,[57] where $\mu = -e\langle i|r|f\rangle$ is the dipole moment associated with the electronic transition. The local photonic density of states in free space is $\rho(\omega) = \omega^2/(\pi^2 c^3)$ [56] and inserting this into Equation 8, we obtain the radiative decay rate of an isolated emitter

$$\gamma_r = \frac{|\mu|^2 \omega^3}{3\pi \varepsilon_0 \hbar c^3}. \tag{9}$$

Remarkably, Equation 9 has exactly the same form as the expression yielded by the Lorentz oscillator for the radiative decay rate of a damped electric dipole in a vacuum,[55] which demonstrates the excellent predictive capabilities of the classical approach.

Let us now consider the specific case of an emitter located closed to a metallic nanoantenna. As we have already anticipated, $\rho(\omega)$ will be strongly altered by its presence. If the nanoantenna supports a LSPR that spectrally overlaps with the emission frequency of the emitter, the LDOS depends on the excitation probability of the plasmonic resonance. In other words, the emitted photons can be emitted into free space or can excite a LSPR. If we restrict our analysis to nanostructures presenting a single mode, this excitation probability can be modeled through a Lorentzian function peaked at the plasmonic resonance, λ_{res}. This allows us to calculate the ratio between the radiative rates of the emitter in the presence, γ_r, and in the absence, γ_{r0}, of the nanoantenna as

$$\frac{\gamma_r}{\gamma_{r0}} = \frac{3}{4\pi^2}\left(\frac{\lambda_{res} Q}{n^3 V}\right), \tag{10}$$

where Q and V are the quality factor and mode volume of the LSPR, respectively, and n is the refractive index of the background medium.[56] This result indicates that nanostructures sustaining modes spectrally narrow and spatially confined lead to large enhancements in the radiative decay rate experienced by any emitter placed close to them. For this reason, metallic NPs are very convenient for manipulating the radiative properties of matter as they provide plasmonic resonances in the optical regime featuring very small (deeply subwavelength) mode volumes, even though typical quality factors are modest. Equation 10 represents the essence of the Purcell effect and the ratio γ_r/γ_{r0} is usually termed as the Purcell factor.

Up to this point, we have discussed how metallic nanostructures improve the radiative properties of already-excited emitters. However, the beneficial effects of metal NPs on the emission properties of matter are not restricted to this. As we already saw in Section 2, they present effective cross sections that can be bigger than their physical size. This property can be used to increase the interaction of any object located in their vicinity with free-space radiation. In the case of fluorescent atoms or molecules close to a nanoantenna, it is well known that the emission intensity is given by the product of two different factors:[45] the emitter quantum yield, η, which measures its ability to radiate once excited, and the electromagnetic energy that it is able to absorb from the electric field in the excitation process, which is proportional to $|\mu E|^2$ (where μ is the transition dipole moment, and E is the electric field evaluated at the emitter position). Thus, we can write the fluorescence enhancement, S, due to the nanoantenna as:

$$S = \frac{\eta}{\eta_0}\frac{|\mu\, E|^2}{|\mu\, E_0|^2}. \tag{11}$$

Two different properties of LSPRs contribute to the fluorescence enhancement. The increase in the ratio $|\mu\ E|^2/|\mu\ E_0|^2$ (where E_0 is the free-space electric field that illuminates the nanoantenna) is related to the capability of plasmonic modes to squeeze and concentrate electromagnetic energy into subwavelength volumes. The quantum yield enhancement, η/η_0, is related to the modification that localized resonances induce in the photonic density of states at the position of the emitter. These two factors can be simultaneously much larger than unity, which leads to strong enhancements of the fluorescence intensity.[29] Note that, rigorously, $|\mu\ E|^2/|\mu\ E_0|^2$ is evaluated at the frequency of excitation, whereas η/η_0 is determined at the frequency of emission. This should be taken into account for the design of efficient plasmonic structures. Thus, a nanoantenna can be cleverly engineered so that it presents a LSPR that matches with the maximum in the absorption spectrum of the emitter and another resonance coinciding with its emission frequency, obtaining both enhancement effects.[57]

Figure 5 shows the experimental confirmation of the Purcell effect in dye molecules close to a nanoantenna[28] consisting of two $90 \times 60 \times 20$ nm^3 gold nanobars (see inset). The antenna is embedded in a nearly homogeneous background medium containing dye molecules. Red circles plot the normalized fluorescence intensity versus time at the resonant frequency of the nanoantenna. In absence of any metal structure, the intensity decay follows an exponential trend from which the decay rate can be extracted, $\gamma_0 \approx 0.3$ ns^{-1}. The presence of the nanoantenna modifies the fluorescence decay of the dye so that it now presents a multiexponential behavior (black squares). Two channels, leading to different decay rates, can be distinguished: a slow decay channel corresponding to the molecules that are far from the antenna, whose decay rate

small NANO MICRO

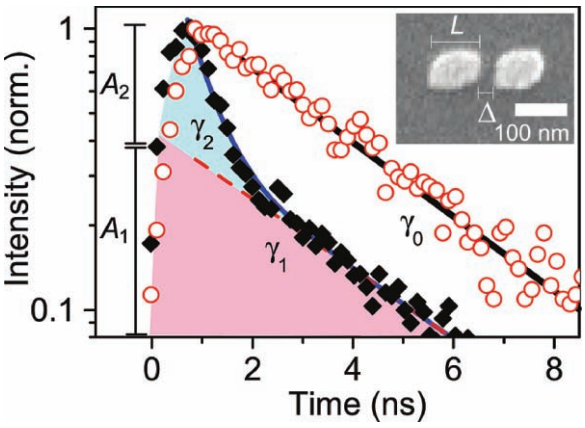

Figure 5. Measurements of normalized fluorescence decay rate of a dye (Atto680, Atto Tec GmbH) near a resonant nanoantenna (black diamonds) and away from the nanoantenna (red open dots) with exponential decay fits (black and blue lines). Inset: SEM image of the resonant gold nanoantenna, consisting of two 90 nm × 60 nm × 20 nm gold nanorods with an antenna gap of 20 nm. Reproduced with permission.[28] Copyright 2007, American Chemical Society.

is very similar to that observed without metallic structures ($\gamma_1 \approx 0.3$ ns^{-1}), and a fast decay rate due to the dyes that, located in the vicinity of the antenna, are strongly coupled to the LSPR that it supports. These molecules must be placed close to the antenna gap (20 nm) and show a decay-rate enhancement bigger than 5 ($\gamma_2 \approx 1.7$ ns^{-1}).

The molecule position and orientation indeed play a relevant role in the fluorescence-enhancement processes as they determine the coupling between the dipole emission and the plasmonic modes of the nanoantenna. This is illustrated in **Figure 6**, which renders FDTD calculations of the yield enhancement, η/η_0, experienced by dye molecules in the vicinity of a gold-bowtie nanoantenna. Figure 6a sketches the different configurations considered. In panel a, the molecule is located at the gap of the antenna, oriented along its axis, which maximizes the coupling to the plasmonic modes of the system. In panel b, the orientation is still parallel to the axis but the position is now out of the gap, and in panel c, the molecule is within the gap but its dipole points along the vertical direction. In each case, three different intrinsic efficiencies, η_0, ranging from 1% to 100% are considered. These results demonstrate how drastic the effects of position and orientation are on the quantum yield enhancement.

Spectra in Figure 6a,b show efficiency maxima whose origins are the electromagnetic fields coupling to the dipole (bright) LSPR that the nanoantenna supports at λ = 630 nm. However, η/η_0 is always below 1 in Figure 6c, developing a sharp minimum (below 10^{-2}) at a slightly larger wavelength (λ = 710 nm). The occurrence of this spectral dip can be related to the fact that, for that polarization, a quadrupolar (dark) mode is efficiently excited in the bowtie antenna, which increases the absorption losses in the system enormously. The insets of the three panels show the electric-field intensity on the same logarithmic scale for the three configurations at resonance. Field plots corroborate the bright and dark nature of the plasmonic modes involved in the different resonant features observed in the spectra. The effects of dark modes can be also observed in the first two panels, where spectra develop minima at λ = 500 nm, which corresponds to the resonant wavelength for the quadrupolar mode that the antenna supports for that polarization.

Remarkably, Figure 6 indicates that the effect of the nanoantenna, even in the most convenient configuration, is only relevant for low-efficiency emitters (blue line) in terms of enhancing quantum yields. For intrinsic quantum yields close to 100% (green line), the presence of the nanoantenna can only worsen the quantum yield of dye molecules and η/η_0 is smaller than unity in all cases. However, FDTD calculations on the scattering properties (plane-wave illumination) of the bowtie antenna considered revealed that, for incident light polarized along the nanoantenna axis, field enhancements at the gap, $|E_{gap}|^2/|E_0|^2$, of the order of 10^3 are obtained at resonance (λ = 650 nm). According to Equation 9, this result implies that enhancements in fluorescence intensity, S, larger than 10^4 or 10^2 can be obtained for low-. or high-efficiency emitters, respectively, located at the gap of the nanoantenna shown in Figure 6. This result is in very good agreement with experimental results on single-molecule fluorescence enhancements near to bowtie antennas recently reported.[29]

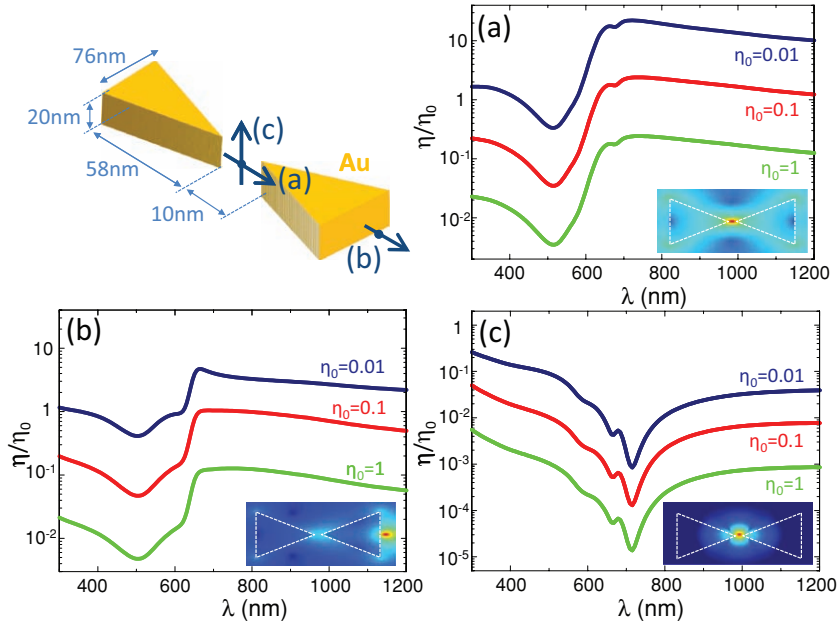

Figure 6. Quantum yield enhancement, η/η_0, for emitters of three different intrinsic efficiencies (η_0) placed in the vicinity of a gold-bowtie nanoantenna. Three different configurations, as sketched in the top right of the figure, are considered: a) the emitter is located at the antenna gap and is oriented parallel to its longest axis; b) the emitter is parallel to the antenna axis and is located 5 nm away from its edge; c) the emitter is situated in the gap of the antenna but is oriented normally to the symmetry plane of the system. Insets: electric-field intensity on the same logarithmic scale for the three configurations at resonance.

5. Outlook and Perspectives

In this Concept article, we have discussed how light can be controlled at the nanoscale using the concept of nanoantennas. The recent improvement of computational capabilities, as well as fabrication and characterization tools, has led to promising work studying and predicting their properties.

We have seen that optical nanoantennas have the ability to squeeze light into very small, subwavelength volumes, particularly in dielectric gaps between two metallic elements. This concentration of the light opens avenues to nonlinear processes and should yield significant improvement of many spectroscopic techniques (Raman scattering, SERS, SEIRA (surface-enhanced infrared absorption), etc.). However, reaching the highest field concentrations/enhancements requires the design of gaps between the metallic elements on the order of a few nanometers. This is still challenging to do in a reproducible way with current technologies and will be necessary to fully take advantage of the potential of those structures.

The understanding of the behavior of the plasmon modes in nanoantennas has improved, thanks to the hybridization concept, leading to the study of dark modes and coherent coupling between plasmonic resonators. Such couplings can lead to Fano resonances or even plasmon-induced transparency. These effects are likely to be useful for sensing applications because of their sharp line shapes or in the design of metamaterials.

The emission properties of nanoemitters can be drastically influenced by the high fields generated by nanoantennas. In the right conditions, radiative decay rates and quantum yields can be increased. The success of this depends strongly on the position and orientation of the emitter compared to the antenna. Still, encouragingly, the best improvement of properties is seen for "bad" emitters, that have low internal quantum efficiency. This means that, via coupling of plasmonic structures to these emitters, a whole new range of materials might become viable for applications. An example is the development of silicon-based emitters, which are of poor quality at the moment, but are easy to process and are compatible with current technology. Indeed, nanoplasmonics is set to open up a bright future for controlled light/matter interactions at the nanoscale.

Acknowledgements

The authors acknowledge funding from the Engineering and Physical Sciences Research Council (EPSRC). V. G. and A. I. F.-D. acknowledge support from the Marie Curie fellowships schemes.

[1] Lord Rayleigh, *Phil. Mag.* **1871**, *107*, 274.
[2] Lord Rayleigh, *Phil. Mag.* **1899**, *41*, 375.
[3] G. Mie, *Ann. Physik* **1908**, *25*, 377.
[4] R. Gans, *Ann. Phys. (Leipzig)* **1912**, *37*, 881.
[5] M. Minsky, "Microscopy apparatus," *US Patent 3013467, Ser. No. 695107*, **1957**.
[6] N. Verellen, Y. Sonnefraud, H. Sobhani, F. Hao, V. V. Moshchalkov, P. Van Dorpe, P. Nordlander, S. A. Maier, *Nano Lett.* **2009**, *9*, 1663–1667.
[7] J. J. Mock, M. Barbic, D. R. Smith, D. A. Schultz, S. Schultz, *J. Chem. Phys.* **2002**, *116*, 6755–6759.
[8] U. C. Fischer, H. P. Zingsheim, *Appl. Phys. Lett.* **1982**, *40*, 195–197
[9] D. W. Pohl, W. Denk, M. Lanz, *Appl. Phys. Lett.* **1984**, *44*, 651–653.
[10] T. Klar, M. Perner, S. Grosse, G. von Plessen, W. Spirkl, J. Feldmann, *Phys. Rev. Lett.* **1998**, *80*, 4249.
[11] A. A. Mikhailovsky, M. A. Petruska, M. I. Stockman, V. I. Klimov, *Optic Lett.* **2003**, *28*, 1686.
[12] G. Ford, W. Weber, *Phys. Rep.* **1984**, *113*, 195–287.
[13] W. L. Barnes, *J. Mod. Opt.* **1998**, *45*, 661.
[14] W. Barnes, A. Dereux, T. Ebbesen, *Nature* **2003**, *424*, 824830.
[15] S. A. Maier, H. A. Atwater, *J. Appl. Phys.* **2005**, *98*, 011101.
[16] P. Mühlschlegel, H. Eisler, O. J. Martin, B. Hecht, D. W. Pohl, *Science* **2005**, *308*, 1607–9.
[17] A. V. Akimov, A. Mukherjee, C. L. Yu, D. E. Chang, A. S. Zibrov, P. R. Hemmer, H. Park, M. D. Lukin, *Nature* **2007**, *450*, 402–406.
[18] S. Maier, *Plasmonics: Fundamentals And Applications*, Springer Verlag, New York **2007**.
[19] P. Bharadwaj, B. Deutsch, L. Novotny, *Adv. Opt. Photon.* **2009**, *1*, 438–483.
[20] J. Lakowicz, Y. Fu, *Laser & Photon. Rev.* **2009**, *3*, 221–232.
[21] W. Murray, W. Barnes, *Adv. Mater.* **2007**, *19*, 3771–3782.
[22] N. C. Lindquist, P. Nagpal, A. Lesuffleur, D. J. Norris, S.-H. Oh, *Nano Lett.* **2010**, *10*, 1369–1373.
[23] T. H. Taminiau, F. D. Stefani, F. B. Segerink, N. F. van Hulst, *Nat. Photon.* **2008**, *2*, 234–237; b) D. K. Gramotnev, S. I. Bozhevolnyi, *Nat. Photon.* **2010**, *4*, 83–91.
[24] G. Vecchi, V. Giannini, J. Gómez Rivas, *Phys. Rev. Lett.* **2009**, *102*, 146807.
[25] J. Kneipp, H. Kneipp, K. Kneipp, *Chem. Soc. Rev.* **2008**, *37*, 1052–1060.
[26] S. Nie, S. R. Emory, *Science* **1997**, *275*, 1102–1106.
[27] K. Kneipp, Y. Wang, H. Kneipp, L. T. Perelman, I. Itzkan, R. R. Dasari, M. S. Feld, *Phys. Rev. Lett.* **1997**, *78*, 1667–1670.
[28] O. Muskens, V. Giannini, J. A. Sanchez-Gil, J. Rivas, *Nano Lett.* **2007**, *7*, 2871–2875.
[29] A. Kinkhabwala, Z. Yu, S. Fan, Y. Avlasevich, K. Mullen, W. E. Moerner, *Nat. Photonics* **2009**, *3*, 654–657.
[30] R. Jin, Y. Cao, C. A. Mirkin, K. L. Kelly, G. C. Schatz, J. G. Zheng, *Science* **2001**, *294*, 1901–1903.
[31] B. J. Wiley, Y. Chen, J. M. McLellan, Y. Xiong, Z. Li, D. Ginger, Y. Xia, *Nano Lett.* **2007**, *7*, 1032–1036.
[32] H. G. Craighead, G. A. Niklasson, *Appl. Phys. Lett.* **1984**, *44*, 1134.
[33] J. R. Krenn, G. Schider, W. Rechberger, B. Lamprecht, A. Leitner, F. R. Aussenegg, J. C. Weeber, *Appl. Phys. Lett.* **2000**, *77*, 3379.
[34] I. Fernandez-Cuesta, R. B. Nielsen, A. Boltasseva, X. Borrisé, F. Pérez-Murano, A. Kristensen, *J. Vac. Sci. Technol. B* **2007**, *25*, 2649.
[35] R. M. Bakker, V. P. Drachev, Z. Liu, H. Yuan, R. H. Pedersen, A. Boltasseva, J. Chen, J. Irudayara, A. V. Kildishev, V. M. Shalaev, *New J. Phys.* **2008**, *10*, 125022.
[36] T. W. Ebbesen, H. J. Lezec, H. F. Ghaemi, T. Thio, P. A. Wolff, *Nature* **1998**, *391*, 667.
[37] L. W. Swanson, *Appl. Surf. Sci.* **1994**, *76–77*, 80–88.
[38] J. Aizpurua, P. Hanarp, D. Sutherland, M. Käll, G. Bryant, F. García de Abajo, *Phys. Rev. Lett.* **2003**, *90*, 5–8.
[39] P. Schuck, D. Fromm, A. Sundaramurthy, G. Kino, W. Moerner, *Phys. Rev. Lett.* **2005**, *94*, 017402.
[40] F. Hao, C. L. Nehl, J. H. Hafner, P. Nordlander, *Nano Lett.* **2007**, *7*, 729–732.
[41] J. Xie, Q. Zhang, J. Y. Lee, D. I. Wang, *ACS Nano* **2008**, *2*, 2473–2480.
[42] V. Giannini, R. Rodríguez-Oliveros, J. A. Sánchez-Gil, *Plasmonics* **2010**, *5*, 99–104.

[43] Y. Sonnefraud, N. Verellen, H. Sobhani, G. A. Vandenbosch, V. V. Moshchalkov, P. Van Dorpe, P. Nordlander, S. A. Maier, *ACS Nano* **2010**, *4*, 1664–70.
[44] P. Ghenuche, S. Cherukulappurath, T. Taminiau, N. van Hulst, R. Quidant, *Phys. Rev. Lett.* **2008**, *101*, 116805.
[45] L. Novotny, *Phys. Rev. Lett.* **2007**, *98*, 266802.
[46] a) M. Schnell, A. García-Etxarri, A. J. Huber, K. Crozier, J. Aizpurua, R. Hillenbrand, *Nat. Photon.* **2009**, *3*, 287–291; b) N. Large, M. Abb, J. Aizpurua, O. Muskens, *Nano Lett.* **2010**, *10*, 1741–1746.
[47] F. Hao, Y. Sonnefraud, P. Van Dorpe, S. A. Maier, N. Halas, P. Nordlander, *Nano Lett.* **2008**, *8*, 3983–3988.
[48] M. Chu, V. Myroshnychenko, C. H. Chen, J. Deng, C. Mou, F. J. García De Abajo, *Nano Lett.* **2009**, *9*, 399–404.
[49] A. L. Koh, K. Bao, I. Khan, W. E. Smith, G. Kothleitner, P. Nordlander, S. A. Maier, D. W. McComb, *ACS Nano* **2009**, *3*, 3015–3022.
[50] E. Prodan, C. Radloff, N. J. Halas, P. Nordlander, *Science* **2003**, *302*, 419–422.
[51] U. Fano, *Phys. Rev.* **1961**, *124*, 1866–1878.
[52] S. Zhang, D. A. Genov, Y. Wang, M. Liu, X. Zhang, *Phys. Rev. Lett.* **2008**, *101*, 047401.
[53] N. Liu, L. Langguth, T. Weiss, J. Kästel, M. Fleischhauer, T. Pfau, H. Giessen, *Nat. Mater.* **2009**, *8*, 758–762.
[54] E. M. Purcell, *Phys. Rev.* **1946**, *69*, 681.
[55] V. Giannini, J. A. Sánchez-Gil, O. L. Muskens, J. G. Rivas, *J. Opt. Soc. Am. B* **2009**, *26*, 1569-1577.
[56] P. R. Berman, *Cavity Quantum Electrodynamics*, Academic Press, San Diego, CA **1994**.
[57] V. Giannini, J. A. Sánchez-Gil, *Opt. Lett.* **2008**, *33*, 899–901.

Received: June 18, 2010
Published online: September 27, 2010

